3D Morpho-Topological Analysis of Asymmetric Neuronal Morphogenesis in Developing Zebrafish

S. Härtel, J. Jara, C.G. Lemus, M.L. Concha
Anatomy and Developmental Biology Program, Faculty of Medicine, Universidad de Chile, Santiago, Chile

ABSTRACT: We applied *in vivo* confocal microscopy of GFP-transgenic zebrafish in combination with 3D image analyses to study the asymmetric morphogenesis of the diencephalic parapineal organ on a supra-cellular, cellular, and sub-cellular level. Following a rough manual segmentation of the respective regions of interest (ROIs), the morphology of generated surface meshes was refined by an active surface model which iteratively adjusts the mesh towards the morphology of the cellular structures. This procedure is essential for a precise morpho-topological analysis, mostly because of the adversarial diffraction limited resolution in the z-dimension of confocal image stacks. 3D Morphology and topology of the reconstructed cellular and supra-cellular structures during morphogenesis was quantified by principal axis transformations and 3D moment invariants. Our data indicates that migration of the parapineal organ is accompanied by a rapid transition between predominantly parallel cell orientations towards predominantly perpendicular orientations, a phenomenon which requires a precise control of cell shape and polarity. The orientational transition is followed by a phase of polarized cell motility in which membrane protrusions in the form of blebs and filopodia become oriented in the direction of the asymmetric migration. The morpho-topological descriptors unveil information that is not perceptible for a direct visual analysis of the microscopical data sets. This approach becomes essential to access morphogenetic mechanisms which control asymmetry and migration.

1 INTRODUCTION

1.1 *Left-right asymmetry in the zebrafish brain*

Despite our increasing understanding of the mechanisms that control left-right asymmetry in the heart, little is known of the morphogenetic mechanisms that establish lateralized circuitry in the vertebrate brain. In recent years we have studied the mechanisms that control the asymmetric development of neuronal nuclei in the zebrafish brain (Concha et al. 2000/2003; Concha 2004). Development of brain asymmetry is preceded by left-sided expression of a number of genes, and is characterized by the allocation of a single midline nucleus on the left side (the parapineal organ), and by left-right differences in the pattern of neuronal differentiation within a paired nucleus (the habenulae). Asymmetric morphogenesis of the parapineal organ is a key event as it induces further asymmetric morphogenesis, and involves the migration of parapineal precursors from their place of origin at the midline towards the left side of the brain (Concha et al. 2003; Gamse et al. 2005). To understand the morphogenetic mechanisms responsible of this phenomenon, we have recently initiated a 3D morphological and topological description of the cell behaviors underlying the asymmetric positioning of the parapineal organ.

1.2 *Morpho-topological analysis of the parapineal organc*

Image processing routines have become indispensable for the reliable detection and quantification of light-microscopic data. Sophisticated algorithms not only restore optical information on the level of data acquisition (see 2.3 below), they become increasingly important for the characterization and quantification of morpho-topological information in biological structures. In the past, we have developed diverse approaches to access biochemical and structure related information on a 2D level (e.g. Carrer et al. 2003; Härtel et al. 2003/2005a/b; Alvarez et al. 2005). In this contribution we continue our approach to reveal biologically relevant information on a 3D level. As shown recently, regulation of cellular volume and morphology can be monitored with great precision in cultured HeLa cells (Castro et al. 2006). In order to derive morpho-topological information

from the parapineal cells and the parapineal organ during the asymmetric morphogenesis in zebrafish embryos, we present an approach based on principle axis transformation and the calculation of rotation, translation, and scale invariant moments. This method has recently been suggested for morphometry of cortical sulci by Mangin et al. (2004). For 3D presentation of cell surfaces and calculation of surface related parameters, we adopt an active surface model introduced by Ahlberg (1996) based on the formulation from Kass et al. (1988). Analytical characterizations are performed on different scales of cellular organization: a supra-cellular scale (pineal and parapineal organ), a cellular scale (parapineal cells), and a sub-cellular scale (blebs and filopodia).

2 MATERIAL & METHODS

2.1 *Manipulation of GFP-transgenic zebrafish*

Transgenic zebrafish expressing green fluorescent protein (GFP) in the dorsal diencephalon were generated previously (Concha et al. 2003), and kept under standard laboratory conditions in the Fish Facility of the Faculty of Medicine, Universidad de Chile. Embryos between 24 and 38 hours post-fertilisation were manually dechorionated, anesthetized with Tricaine (3-amino benzoic acid ethy lester, Sigma), and mounted in a custom-made chamber in 1% agarose dissolved in embryo medium (Concha et al. 2003). After the end of the experiment, embryos were removed from the chamber and sacrificed with a Tricaine overdose.

2.2 *Acquisition of confocal microscopic images*

The morphogenesis of the parapineal organ in living GFP-transgenic zebrafish embryos was followed by confocal epifluorescence microscopy (Leica TCS SP) under controlled temperature conditions (28°C). 3D Image stacks, intensity $I \in [0, 255]$, were captured with a 63x (NA 0.9) water-immersion objective, excitation/emission at 488/505–560 nm, with typical xyz stack [512 × 512 × 70 voxels] and voxel [0.116 × 0.116 × 0.5 µm/voxel] dimensions. The selected vertical sampling distances guaranteed reliable volume determinations and shape analysis.

2.3 *Deconvolution and image analysis*

Huygens Scripting (Scientific Volume Imaging BV, www.svi.vl, Hilversum, Netherlands), using a Maximum Likelihood Estimator (MLE) algorithm was used to deconvolve 3D confocal data in order to reveal hidden details of the biological structures and to improve the signal to noise ratio significantly. All further image processing routines for visualization and morpho-topological analysis were written in our laboratory, using Interactive Data Language (IDL, ITT, www.ittvis.com/idl/, CO, USA).

2.4 *Cell segmentation and surface reconstruction*

A first approximation of ROIs including sub-cellular structures (blebs or filopodia) and parapineal cells was obtained manually by drawing object contours into the xy-frames of the deconvolved image stacks, using an Interactive Pen Display (Cintiq-15X, Wacom). Binary masks of the ROI were generated with a custom-made macro written for the public domain image analysis software Image-SXM (http://www.liv.ac.uk/~sdb/imageSXM). The definition of cellular contours in 3D was improved significantly by the application of a modified version of an active surface model that was originally presented by Ahlberg (1996) expanding the 2D active contour model developed by Kass et al. (1988). The active surface model parameterizes internal forces like elasticity (α) or rigidity (β), which counteract line tension or curvature and mimic intrinsic physical properties of a deformable surface.

Following Xu & Prince (1998), surface tension and curvature are induced by external force fields, which are derived from the intensity gradients and laplacians of the image data by an iterative algorithm. The external forces are parameterized by so-called Generalized Gradient Vector Flows (GGVF) and consist of 3D vector fields, which attract surface points towards the object borders. Force balance between internal and external forces is solved by the Euler-Lagrange condition for the minimization of an energy functional E for a parametric surface $\underline{C}(s) = [x(s), y(s), z(s)]$, $s \in [0,1]$.

$$E = \int_0^1 0.5 \cdot [\alpha |\underline{C}'(s)|^2 + \beta |\underline{C}''(s)|^2] + E_{ext}(\underline{C}(s))ds \qquad [1]$$

For the cellular structures presented in this work, an initial surface mesh is derived from the manually approximated ROI contours.

Precise assimilation of the active surface mesh towards the morphology of the cellular structures was supervised interactively by setting the appropriate parameter combination to the following coefficients: α, β, viscosity (γ), external force (k) and iterations (t).

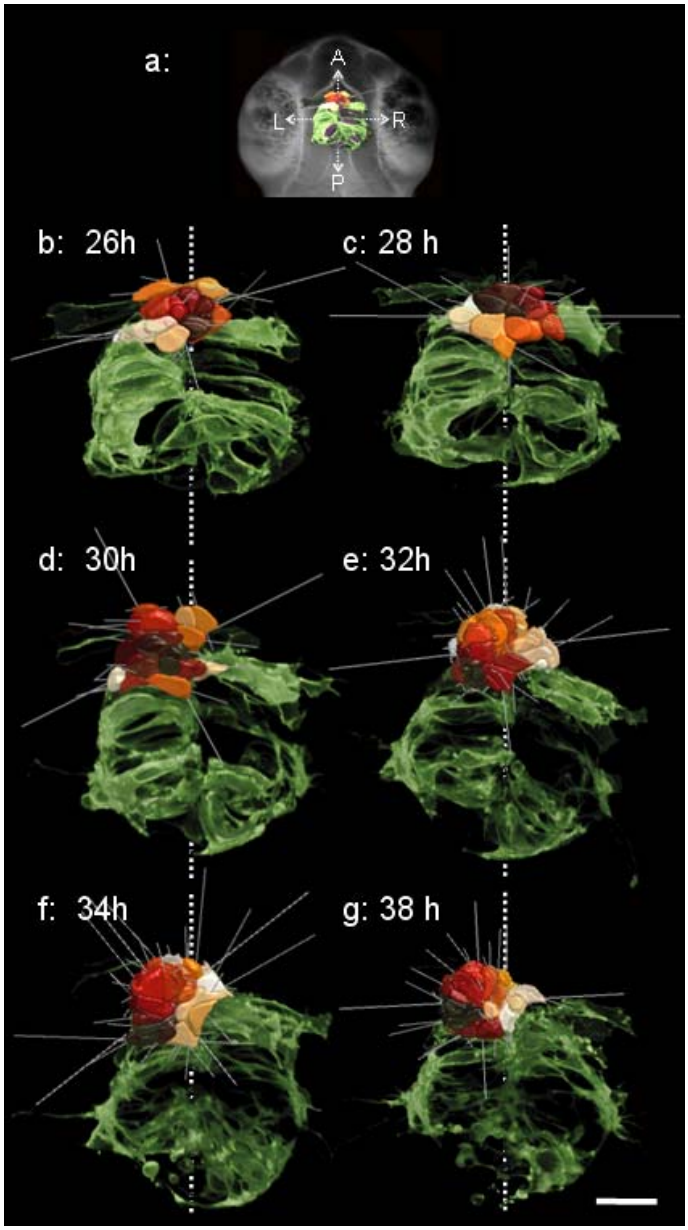

Figure 1. Topological reorganization of the parapineal organ during asymmetric morphogenesis. [a] Scheme shows the transparent head of a developing fish embryo and the fluorescence of the GFP-transgenic pineal complex (green). The parapineal organ is located at the anterior-most end of this complex. [b-g] Pineal complex (green) and colour-coded active surface models of individual cells of the parapineal organ at 26, 28, 30, 32, 34, and 38 hours post-fertilisation. Left-right symmetry axes of the pineal complex are shown by dotted, vertical lines. Thick and thin grey lines depict principal axes of the entire parapineal organ and of individual reconstructed cells, respectively. Abbreviations: anterior (A), posterior (P), left (L), right (R). Scale bar = 20µm.

2.5 *Calculation of surface curvature*

Surface curvature (κ) was calculated for each mesh node in respect to its adjacent neighbours. For this purpose spheres with radius ($r = \kappa^{-1}$) were fitted to each node and 3 of its neighbours. For nodes with more than 3 neighbours, we calculate κ for all possible 3 neighbour combinations and derived a mean value for κ.

2.6 *Invariant moments*

Eigen vectors ($\underline{e}_{1,2,3}$) and Eigen values ($\lambda_{1,2,3}$) of segmented objects were calculated on three levels of spatial organization: *(i)* on the sub-cellular level (blebs and filopodia, ∅ = 1-3 µm), *(ii)* on the cellular level (individual parapineal cells, ∅ = 5-15 µm), and *(iii)* on the supra-cellular level (parapineal organ, ∅ = 20-100 µm). Eigen vectors and values were derived from the inertia tensor T (or covariance matrix) by Householder reduction and the QL method (based on the routine `tqli` described by Press et al. 1992). T is required in order to determine the rotation of a rigid body around its centre of mass. In analogy to mechanical physics, the segmented structures were considered to have a uniform mass distribution ρ(x,y,z) = 1 in each segmented voxel. The Eigen values and vectors were ordered in respect to the size of λ_i, which directly represents the rotational inertia in respect to each axis $\underline{e}_i$. The Eigen systems $\underline{E} = [\lambda_1 \cdot \underline{e}_1, \lambda_2 \cdot \underline{e}_2, \lambda_3 \cdot \underline{e}_3]$ were used to access object morphologies (morphometry), spatial orientation between objects of the same level of organization (Fig. 1), and spatial organization between the different levels of organization (Fig. 2). In addition, segmented parapineal cells were transformed into their corresponding Eigen systems ρ(x,y,z) → ρ(x',y',z') and aligned in box pattern in order to improve the visual perception of more subtle geometric features.

Object morphometry was parameterized by translation-, rotation-, and scale-invariant descriptors (μ'_{ijk} invariant moments of order ijk), which were calculated according to Castleman (1996):

$$\mu_{ijk} = \int_{-\infty}^{\infty}\int_{-\infty}^{\infty}\int_{-\infty}^{\infty}(x'-\bar{x})^i (y'-\bar{y})^j (z'-\bar{z})^k \rho(x',y',z')dx'dy'dz' \quad [2]$$

$$\mu'_{ijk} = \mu_{ijk} / \mu_{000}^{((i+j+k)/3)+1} \quad [3]$$

3 RESULTS

Fig. 1 shows a temporal series of 3D reconstructions in which the topological reorganization of the parapineal organ is depicted at supra-cellular and cellular levels. The initial phase of asymmetric migration is revealed as a gradual movement of the parapineal organ to the left in respect to the mayor symmetry axis of the entire pineal complex. This phenomenon is accompanied by oscillations in the orientation of the 1st principal axis of the parapineal organ and by changes in the orientation of the 1st principal axes of individual parapineal cells: at early stages principal axes show a predominantly parallel

alignment, which is gradually lost during morphogenesis.

Fig. 2 shows a quantitative analysis of the temporal reorganization of the alignments of the 1st principal axes of the parapineal cells in respect to each other (red circles) and in respect to the 1st principal axes of the entire parapineal organ (white squares), which accompanies the asymmetric cell migration described in Fig. 1. Both parameters indicate a reorganization of a predominantly parallel axes alignment (26-28 h post-fertilization) towards a predominantly perpendicular alignment (32-38 h), undergoing an intermediate phase of random distribution (30 h). The transition between the parallel alignment toward the predominantly perpendicular orientation between the principal axes of individual cells and the axis of the entire parapineal organ occurs within a time span of 2-4 h.

Further information about the process of reorganization during the orientational transition presented in Fig. 2 was obtained by a more detailed analysis of the distribution of the angles between the 1st principal axes of individual parapineal cells. Fig. 3 connects the spatial allocation within the 3D reconstructions with the parameter distribution of a sample population that enters the phase of orientational transition (28 h).

As can be observed, cells with a predominantly parallel axes alignment form the left wing of the

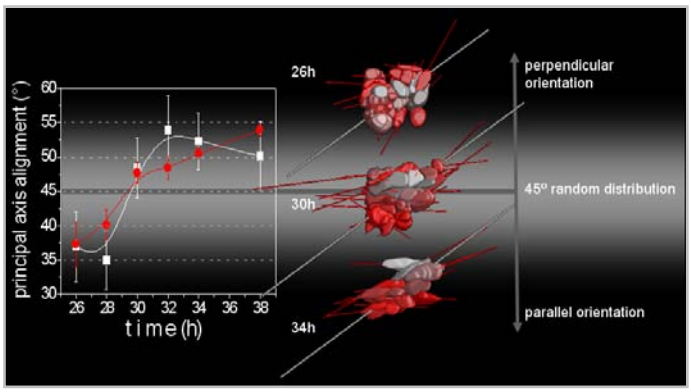

Figure 2. Principal axes alignment during parapineal morphogenesis. [Left] Alignment between the 1st principal axis of individual parapineal cells (red circles) is compared to the alignment between the 1st principal axis of the individual cells with the 1st principal axis of the entire parapineal organ (white squares). The parameter 'principal axis alignment' represents the mean values calculated from the respective angular distributions in three independent experiments. Mean values were connected by β-spline curves. Error bars represent standard deviations. [Centre-Right] Representative surface reconstructions of the parapineal organ based on active contours in combination with the respective 1st principal axis of individual parapineal cells (red lines) and of the entire parapineal organ (grey lines) at 26, 30, and 34 hours post-fertilisation. The reconstructions open a direct visual access to the data presented in the plot. The data reveals a transition of the organization of parapineal cells from a predominantly parallel orientation towards predominantly perpendicular orientation.

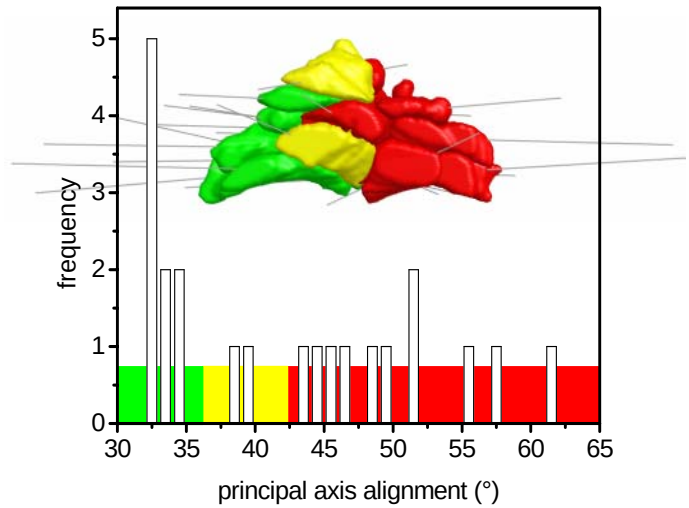

Figure 3. Asymmetric distribution of the axial alignment of parapineal cells during morphogenesis. The histogram plots the frequency distribution of the parameter 'inter cellular alignment of the 1st principal axis ($\underline{e}_1$)' for a representative parapineal cell population at 28 h post fertilisation. Three intervals of the angular alignment were colour coded according to the predominant orientation: parallel (green), random (yellow), and perpendicular (red) (see Fig. 2). Colours were projected to the surface of the corresponding parapineal cells.

parapineal organ (green), while cells that diverge from the parallel alignment constitute the right wing of the organ (red). In addition, cells with an intermediate degree of alignment are located close to the centre (yellow).

On a final level of 3D topological analysis, we analysed the distribution of sub-cellular structures (membrane protrusions) within cells of the parapineal organ. Fig. 4 visualizes the sub-cellular structures for a wild type and a mutant embryo and shows the spatial distribution of membrane protrusions in the form of blebs (red) and filopodia (yellow). In the wild type, parapineal membrane protrusions show a polarised behaviour during the asymmetric morphogenesis as they concentrate on the left side to which the parapineal organ migrates. In constrast to the wild type, protrusion polarisation is lost in a mutant embryo that is characterized by an impaired parapineal migration.

4 DISCUSSION

Principal axes transformation and invariant moments have been introduced a few decades ago for the characterisation and recognition of pattern in 2D images by Hu (1962), and for the analysis of 3D data sets by Lo & Don (1989). The method presents a standard mathematical tool that is applied in a wide range of disciplines including statistics, quantum mechanics, or classical mechanics. In biological and medical science however, the application of this attractive tool is rather sparse.

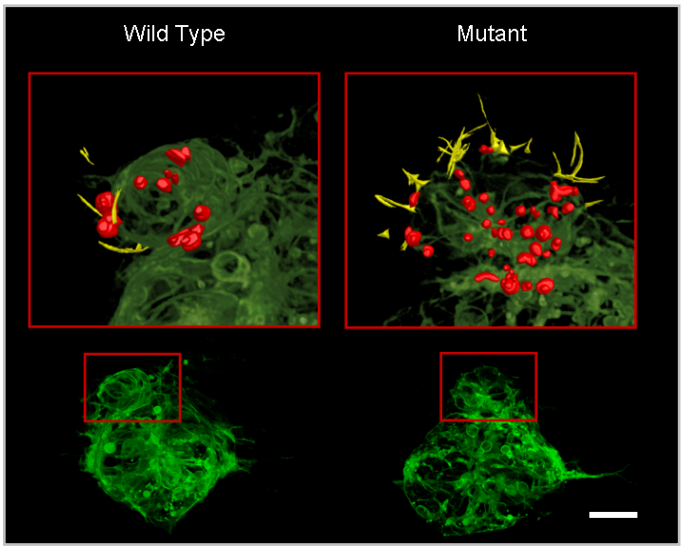

Figure 4. Spatial distribution of sub-cellular structures within the parapineal organ of wild type (left) and mutant (right) zebrafish embryos. As can be observed in the upper 3D reconstructions, membrane protrusions in the form of blebs (red), and filopodia (yellow) are oriented in the direction of the asymmetric migration toward the left side of the wild type pineal complex. In contrast, blebs and filopodia are symmetrically oriented in the mutant. Scale bar = 20µm.

Recently, 3D invariant moments have been reported to provide good discriminatory power to identify handedness- and sex-correlated shapes of the cortical sulci in brain morphometry (Mangin et al. 2004). The general low acceptance of invariant moments in biological and medical science might be caused by the slightly abstract formalism (see [2,3]). Nevertheless, the invariants up to the power of 2 have a direct physical relevance: they define the principal rotational axis of a solid body of homogeneous or heterogeneous mass distribution ($\rho(x,y,z) = 1$ or $\rho(x,y,z) = f(x,y,z)$).

The calculated Eigen system $\underline{E} = [\lambda_1 \cdot \underline{e}_1, \lambda_2 \cdot \underline{e}_2, \lambda_3 \cdot \underline{e}_3]$ directly presents the rotational symmetry axes ($\underline{e}_{123}$, axes where the angular momentum is unchanged, unless an external torque is applied) in combination with its respective rotational inertia (λ_{123}). Length and orientation of projected axes ($\lambda_i \cdot \underline{e}_i$) therefore represent and quantify an essential visual characteristic of a solid body or cellular surface (see Fig. 1-3): the longest principal axis ($\lambda_1 \cdot \underline{e}_1$) generally aligns with the elongated axis of a cellular body.

Principal axes become explicitly powerful when it comes to characterize the orientation of individual cells which form a complex supra-cellular structure. In case of the developing parapineal organ, an agglomeration of 15-20 cells already makes it difficult to visually explore the orientation of each individual cell (see Fig. 1-3). Therefore the morpho-topological descriptors unveil information that is not perceptible for a direct visual analysis of the microscopical data sets. For example, the transition of the orientational organisation within the parapineal organ could not be perceived visually without the projection of the principal axes (Fig. 1).

The rapid access to statistical properties of the axes components on a cellular and a supra-cellular level permitted to determine the temporal interval for the orthogonal transition in parapineal cell organisation (Fig. 2). Finally, the back projection of colour coded parameter intervals revealed a supra-cellular pattern inside the parapineal organ (Fig. 3). Altogether, the analysis allowed us to detect a morphogenetic asymmetry prior to the lateral migration of the organ (compare 28 h and 30 h in Fig. 1 with Fig. 3). The detected internal cellular pattern directly leads to the question of the underlying biological mechanisms.

In conclusion, a relatively simple mathematical analysis unveils new biological questions in respect to the first phenomena of asymmetry during parapineal morphogenesis. We are presently expanding the analysis in all levels of organization and include mutant zebrafish embryos (Fig. 4) to address the biological implication of the observed phenomena.

5 REFERENCES

Ahlberg, J. 1996. Active Contours in Three Dimensions. Thesis project done at Computer Vision Laboratory, Linköping University, Sweden.

Alvarez, M.; Godoy, R.; Heyser, W. & Härtel, S. 2005. Anatomical-physiological determination of surface bound phosphatase activity in ectomycorrhiza of Nothofagus obliqua based on image processed confocal fluorescence microscopy. *Soil Biology and Biochemistry* 37(1): 125-132.

Castleman, K.R. 1996. *Digital Image Processing*. Prentice Hall, Englewood Cliffs, NJ, USA.

Castro, J.; Ruminot, I.; Porras, O.; Flores, C.; Hermosilla, T.; Verdugo, E.; Härtel, S. & Barros, L.F. 2006. ATP steal: a novel mechanism linking Na+ with the onset of necrotic Ca2+ overload. In press: *Cell Death & Differentiation*.

Carrer, D.; Härtel, S. & Maggio, B. 2003. Ceramide Modulates the Lipid Membrane Organization at Molecular and Supramolecular Levels. *Chemisty and Physics of Lipids* 122: 147-152.

Concha, M.L.; Burdine, R.D.; Russel, C.; Schier, A.F. & Wilson, S.W. 2000. A Nodal signalling pathway regulates the laterality of neuroanatomical asymmetries in the zebrafish forebrain. *Neuron* 28: 399-409.

Concha, M.L.; Russell, C.; Regan, J.C.; Tawk, M.; Sidi, S.; Gilmour, D.; Kapsimali, M.; Sumoy, L.; Goldstone, K.; Amaya, E.; Kimelman, D.; Nicolson, T.; Grunder, S.; Gomperts, M.; Clarke, J.D. & Wilson, S.W. 2003. Local tissue interactions across the dorsal midline of the forebrain establish CNS laterality. *Neuron* 39: 423-438.

Concha, M.L. 2004. The dorsal diencephalic conduction system of zebrafish as a model of vertebrate brain lateralisation. *Neuroreport* 15: 1843-1846.

Gamse, J.T.; Kuan, Y.S.; Macurak, M.; Brosamle, C.; Thisse, B.; Thisse, C.; & Halpern, M.E. 2005. Directional asymme-

try of the zebrafish epithalamus guides dorsoventral innervation of the midbrain target. *Development* 132: 4869-4881.

Härtel, S.; Zorn-Kruppa, M.; Tykhonova, S.; Alajuuma, P.; Engelke, M. & Diehl, H. 2003. Staurosporine-Induced Apoptosis in Human Cornea Epithelial Cells In Vitro. *Cytometry* 08, 15-23.

Härtel, S.; Fanani, M.L.; & Maggio, B. 2005a. Shape transitions and lattice structuring of ceramide-enriched domains generated by sphingomyelinase in lipid monolayers. *Biophysical Journal* 88: 287-304.

Härtel, S.; Rojas, R.; Räth, C.; Guarda, M.I. & Goicoechea, O. 2005b. Identification and Classification of Di- and Triploid Erythrocytes by Multi-parameter Image Analysis: A New Method for the Quantification of Triploidization Rates in Rainbow Trout (Oncorhynchus mykiss). *Archivos de Medicina Veterinaria* 37(2): 147-154.

Hu, M.K. 1962. Visual pattern recognition by moment invariants. *IRE Transactions on Information Theory* 8 (February): 179–187.

Kass, M.; Witkin, A. & Terzopoulos, D. 1988. Snakes: Active Contour Models. *International Journal of Computer Vision* 1: 321-331.

Lo, C.-H. & Don, H.S. 1989. *3D moment forms: their construction and application to object identification and positioning*. *IEEE PAMI 11* (October): 1053–1064.

Mangin J.F.; Poupon, F.; Duchesnay, E.; Riviere, D.; Cachia A.; Collins, D.L.; Evans, A.C. & Regis J. 2004. *Brain morphometry using 3D moment invariants.* Medical Image Analysis 8: 187–196.

Press, W.H.; Teukolsky, S.A.; Vetterling, W. & Flannery, B.P. 1992. *Numerical Recipes in C: The Art of Scientific Computing* (2nd edition), section 11.3, Cambridge University Press.

Xu, C. & Prince, J.L. 1998. Generalized gradient vector flow external forces for active contours. *Signal Processing* 71: 131-139.

6 ACKNOWLEDGEMENTS

This work was supported by FONDECYT 1060890, PBCT ACT 47, and ICM P04-068-F.